Polyhedron 58 (2013) 71–78

Contents lists available at SciVerse ScienceDirect

Polyhedron

journal homepage: www.elsevier.com/locate/poly

Oxidative reactivity and cytotoxic properties of a platinum(II) complex prepared by outer-sphere amide bond coupling

Justin J. Wilson, Stephen J. Lippard *

Department of Chemistry, Massachusetts Institute of Technology, Cambridge, MA 02139, United States

ARTICLE INFO

Article history:
Available online 17 August 2012

This article is dedicated to the memory of Michelle Millar, a wonderful friend, colleague, and scientist.

Keywords:
Cisplatin
MTT assay
X-ray crystallography
NMR spectroscopy
Amide coupling
Platinum

ABSTRACT

Benzyl amine was coupled to the dangling carboxylic acid groups of the platinum(II) complex [Pt(edda)Cl_2], where edda = ethylenediamine-*N*,*N*′-diacetic acid, to give the diamide-tethered complex [Pt(L)Cl_2] (**1**), where L = ethylenediamine-*N*,*N*′-bis(*N*-benzylacetamide). Complex **1** was oxidized with both $PhICl_2$ and Br_2. Oxidation with $PhICl_2$ cleanly afforded the tetrachloride complex, [Pt(L)Cl_4] (**2**), whereas oxidation with Br_2 gave rise to several mixed halide complexes of the general formula, [Pt(L)Cl_x-Br_{4-x}], where x = 1, 2, or 3. Complexes **1** and **2** were fully characterized by ^{1}H, ^{13}C, and ^{195}Pt NMR spectroscopy, as well as by ESI-MS. These compounds exist as a mixture of diastereomers that arise from the chirality of the two coordinated nitrogen atoms. Crystal structures of **1**, **2**, and [Pt(L)Cl_xBr_y] (**3**) are reported. Although refined as the tetrabromide complex [Pt(L)Br_4], the crystal structure of **3** is a mixture of species with site-occupancy disorder of chloride and bromide ligands. DFT calculations indicate that the two sets of diastereomers of **1** and **2** are effectively thermoneutral, a conclusion that is also supported by the observation of both members of each pair by NMR spectroscopy. The cytotoxicity of **1** and **2** was measured by the MTT assay in HeLa cells and compared to that of cisplatin. Both exhibit IC_{50} values close to 50 μM and are therefore substantially less toxic than cisplatin, for which the IC_{50} is 1 μM.

1. Introduction

Cisplatin is a widely used and effective metal-based chemotherapeutic agent. The biological properties of this simple coordination compound were discovered in 1965, leading to subsequent FDA-approval for the treatment of testicular and bladder cancer in 1978 [1]. Since then, a wide array of platinum complexes have been synthesized and tested for biological activity with the goal of finding new platinum-based chemotherapeutics with fewer toxic side effects and a different spectrum of activity [2]. The two approved second-generation compounds, carboplatin and oxaliplatin, are one result of this research endeavor. Despite the clinical success of these three compounds, their side effects [3,4] and lack of efficacy in certain cancer types, primarily due to resistance [5], drives the search for new platinum-based anticancer agents.

The ability to systematically modify potential platinum anticancer agents by predictable and readily controlled chemistry is of value for the synthesis of new drug candidates having novel properties. In recent years, this principle has been applied to generate platinum(IV) prodrugs. For example, the free carboxylic acid groups of the platinum(IV) compound *cis*,*cis*,*trans*-[Pt(NH_3)$_2$$Cl_2$(succinate)$_2$] can engage in amide bond coupling reactions [6]. Functionalization of this compound via amide bond formation has led to the synthesis of many new platinum(IV) complexes that were tested for biological activity [6–11]. This predictable chemistry has also been used to attach platinum(IV) prodrugs to peptides [12–15] and various nano-delivery devices [16–21] for improved anticancer efficacy.

Previously, we reported an analogous amide bond coupling reaction using the dangling carboxylic acid of the platinum(II) complex [Pt(edma)Cl_2], where edma = ethylenediamine-*N*-monoacetic acid [22]. This chemistry was used to tether a dansyl fluorophore on the ethylenediamine backbone of the platinum(II) complex. The resulting complex behaved as a fluorescent reporter for the oxidation state of the platinum center, thus demonstrating the potential utility of this chemistry for designing complexes with valuable properties. In the present article we describe amide bond formation on the platinum(II) complex, [Pt(edda)Cl_2] where edda = ethylenediamine-*N*,*N*′-diacetic acid having two free carboxylic acid groups. Oxidation of this new platinum(II) complex by $PhICl_2$ and Br_2 was investigated, together with the cytotoxic properties of the two chloride complexes in HeLa cells.

2. Experimental

2.1. General considerations

All reactions were carried out under normal atmospheric conditions. Solvents were used as received without additional drying or

* Corresponding author. Tel.: +1 (617) 253 1892; fax: +1 (617) 258 8150.
E-mail address: lippard@mit.edu (S.J. Lippard).

0277-5387/$ - see front matter © 2012 Elsevier Ltd. All rights reserved.
http://dx.doi.org/10.1016/j.poly.2012.07.097

purification. The compounds, [Pt(edda)Cl_2] (edda = ethylenediamine-*N*,*N*′-diacetic acid) [23] and iodobenzene dichloride [24], were synthesized as previously described. Benzylamine and carbonyldiimidazole (CDI) were purchased from Sigma Aldrich and used as received.

2.2. Physical measurements

NMR spectra were recorded on a Bruker DPX-400 or Varian Mercury spectrometer in the MIT Department of Chemistry Instrumentation Facility at 20 °C. ^{1}H and ^{13}C{^{1}H} NMR spectra were referenced internally to residual solvent peaks, and chemical shifts are expressed relative to tetramethylsilane, $SiMe_4$ (δ = 0 ppm). ^{195}Pt{^{1}H} NMR spectra were referenced externally to K_2PtCl_4 in D_2O (δ = −1628 ppm). Electrospray ionization mass spectra (ESI-MS) were acquired on an Agilent Technologies 1100 series LC-MSD trap. ESI-MS and NMR spectra of all compounds are given in the Supplementary data (Figs. S1–S10). Fourier transform infrared (FTIR) spectra were recorded with a ThermoNicolet Avatar 360 spectrometer running the OMNIC software. Samples were prepared as KBr disks. Melting points were obtained on a Meltemp apparatus and are reported uncorrected. X-ray powder diffraction data were obtained using a Bruker D8 Advance diffractometer equipped with a Cu Kα radiation source. The sample was placed on a rotating stage, and data were acquired at every 0.01° at a rate of 0.2 s/step.

2.3. Synthesis of [Pt(L)Cl_2] (**1**)

A solution of CDI (0.465 g, 2.87 mmol) in 50 mL of DMF was added to a suspension of [Pt(edda)Cl_2] (0.619 g, 1.40 mmol) in 16 mL of DMF. The resulting mixture was heated at 60 °C for 10 min, at which point a yellow solution resulted, and then sparged with N_2 for 5 min. Benzylamine (0.307 g, 2.87 mmol) in 40 mL of DMF was added in a dropwise manner to this solution containing the activated platinum complex. After stirring for 12 h, the solution was concentrated to 15 mL under reduced pressure and elevated temperature (60 °C). The addition of 20 mL of water afforded the desired compound as an off-white solid, which was isolated by filtration and washed sequentially with 5 mL of water, 2 × 5 mL of ethanol, and 2 × 5 mL of diethyl ether (Et_2O) before being dried in vacuo. Yield: 0.594 g (68%). M.p. > 280 °C (gradual browning), 302–307 °C (dec into black liquid). ^{1}H NMR (400 MHz, DMF-d_7): *R*,*R*/*S*,*S* + *R*,*S* diasteromers (1:1) δ 8.64 (2H, two overlapping triplets, amide NH), 7.36–7.24 (multiplet, 10H, aromatic protons), 6.22 + 6.15 (2H, broad singlets, coordinating NH), 4.48–4.38 (m, 4H, benzyl CH_2), 4.31–4.16 (2H, two doublets, CH adjacent to amide), 3.80–3.62 (two doublet of doublets, 2H, CH adjacent to amide), 3.21–3.11 (broad multiplet, 2H, CH_2 ethylenediamine backbone), 2.72–2.66 (broad multiplet, 2H, CH_2 ethylenediamine backbone). ^{13}C{^{1}H} NMR (100 MHz, DMF-d_7): *R*,*R*/*S*,*S* + *R*,*S* diasteromers (1:1) δ 168.1 + 168.0, 139.50 + 139.48, 128.7, 127.82, 127.79, 127.3, 55.6 + 54.7, 55.1, 42.91. ^{195}Pt{^{1}H} NMR (86 MHz, DMF-d_7): *R*,*R*/*S*,*S* + *R*,*S* diasteromers (1:1) δ −2347, −2362. IR (KBr, cm^{-1}): 3340 m, 3165 m, 3111 m, 2949 w, 1685 m, 1662 s, 1555 m, 1496 w, 1452 w, 1419 m, 1358 w, 1261 m, 1078 w, 1025 w, 986 w, 860 w, 748 w, 695 w, 581 w, 453 w. ESI-MS (negative-ion mode): *m*/*z* 582.9 ([$PtLCl_2$–2H–Cl]$^-$, Calc. 583.1), 619.0 ([$PtLCl_2$–H]$^-$, Calc. 619.1), 1239.1 ([2$PtLCl_2$–H]$^-$, Calc. 1239.2). *Anal.* Calc. for $C_{20}H_{26}Cl_2N_4O_2Pt$: C, 38.72; H, 4.22; N, 9.03. Found: C, 38.71; H, 4.13; N, 8.96%.

2.4. Synthesis of [Pt(L)Cl_4] (**2**)

To a suspension of **1** (200 mg, 0.322 mmol) in 5 mL of DMF, a solution of $PhICl_2$ (91 mg, 0.33 mmol) in 1 mL of DMF was added in a dropwise manner. The suspension became a bright yellow solution, which was allowed to stir at rt for 1 h. The solution was filtered and 200 mL of Et_2O was added. After 10 min, a fine yellow solid deposited. This solid was isolated by vacuum filtration, washed twice with 10 mL of Et_2O, and then dried under vacuum. Yield: 0.108 g (49%). M.p. > 200 °C (gradual browning), 255–265 °C (dec into black char). ^{1}H NMR (400 MHz, DMF-d_7): *R*,*R*/*S*,*S* + *R*,*S* diasteromers (3:1) δ 8.95 + 8.92 (triplets, 2H, NH amide), 7.39–7.28 (overlapping multiplets, 12H, 5H aromatic + NH), 4.50 + 4.45 (doublets, 4H, benzyl CH_2), 4.23–3.80 (multiplets, 4H, CH_2 adjacent to amide), 3.60–3.20 (broad multiplets, 4H, CH_2 ethylenediamine backbone). ^{13}C{^{1}H} NMR (100 MHz, DMF-d_7): *R*,*R*/*S*,*S* + *R*,*S* diasteromers (3:1) δ 166.6 + 166.5, 139.2 + 139.1, 128.7, 127.8, 127.4, 57.4 + 57.2, 55.0 + 54.3, 43.3 + 43.2. ^{195}Pt{^{1}H} NMR (86 MHz, DMF-d_7): *R*,*R*/*S*,*S* + *R*,*S* diasteromers (3:1) δ −370 (minor), −378 (major). IR (KBr, cm^{-1}): 3440 m, 3294 m, 3153 w, 3105 w, 2924 w, 2876 w, 1657 s, 1584 w, 1571 m, 1495 vw, 1450 w, 1384 w, 1410 w, 1324 w, 1277 w, 1216 vw, 1068 w, 758 m, 704 m, 508 w. ESI-MS (negative-ion mode): *m*/*z* 580.9 ([$PtLCl_4$–4H–3Cl]$^-$, Calc. 581.1), 616.9 ([$PtLCl_4$–3H–2Cl]$^-$, Calc. 617.1), 652.9 ([$PtLCl_4$–2H–Cl]$^-$, Calc. 653.1), 689.0 ([$PtLCl_4$–H]$^-$, Calc. 689.0), 1381.1 ([2$PtLCl_4$–H]$^-$, Calc. 1380.9). *Anal.* Calc. for $C_{20}H_{26}Cl_4N_4O_2$-Pt: C, 34.75; H, 3.79; N, 8.10. Found: C, 34.70; H, 3.66; N, 8.20%.

2.5. Oxidation of **1** with Br_2

To a suspension of **1** (115 mg, 0.185 mmol) in 3 mL of DMF was added Br_2 in DMF (0.61 M, 460 μL, 0.28 mmol). The mixture was left to stir at rt in the absence of light for 0.5 h. The resulting orange solution was filtered and set up for vapor diffusion with water as the entering solvent. After 6 days, orange microcrystalline material deposited. The supernatant was decanted and the remaining solid was washed with 3 × 5 mL water, 2 × 5 mL EtOH, and 2 × 5 mL Et_2O sequentially, prior to drying in vacuo. This material, as described below in Sections 3.3 and 3.4, is composed of a mixture of platinum(IV) compounds with the general formula [Pt(L)Cl_{x}-Br_{4-x}], where *x* is a positive integer ≤3. Yield: 109 mg. ESI-MS (negative-ion mode): *m*/*z* 581.0 ([$PtLCl_2Br_2$–Cl–2Br–4H]$^-$, Calc. 581.1), 619.0 ([$PtLCl_2Br_2$–2Br–3H]$^-$, Calc. 617.1), 625.0 ([$PtLCl_2Br_2$–2Cl–Br–4H]$^-$, Calc. 625.1). 660.9 ([$PtLCl_2Br_2$–Cl–Br–3H]$^-$, Calc. 661.0), 698.8 ([$PtLCl_2Br_2$–Br–2H]$^-$, Calc. 697.0 (100%), 699.0 (99.1%)), 706.8 ([$PtLCl_2Br_2$–2Cl–3H], Calc. 707.0), 734.8 ([$PtLCl_3Br$–H]$^-$, Calc. 735.0), 742.8 ([$PtLCl_2Br_2$–Cl–2H]$^-$, Calc. 743.0), 778.8 ([$PtLCl_2Br_2$–H]$^-$, Calc. 778.9), 822.7 ([$PtLClBr_3$–H]$^-$, Calc. 822.9), 904.7 ([$PtLClBr_3$+Br] or [$PtLBr_4$+Cl], Calc. 904.8).

2.6. Theoretical calculations

DFT calculations were carried out with the *ORCA* program package [25]. Geometries were optimized in the gas-phase using the BP86 functional [26–28]. The def2-TZVP(-f) basis set and the decontracted def2-TZVP/J auxiliary basis set were used for all atoms with the zeroth-order regular approximation (ZORA) to account for relativistic effects [29,30]. Numerical frequency calculations at the same level of theory revealed the optimized geometries to be local minima on the potential energy surface and were used for thermodynamic calculations.

2.7. X-ray crystallographic studies

Single crystals were mounted in Paratone oil on cryoloops and frozen under a 100 K KRYO-FLEX nitrogen cold stream. In general, data were collected on a Bruker APEX CCD X-ray diffractometer with graphite-monochromated Mo Kα radiation (λ = 0.71073 Å) controlled by the *APEX2* software package [31]. For **2** and **3**, absorption corrections were applied using *SADABS* [32]. The structures were solved using direct methods and refined on F^2 with the *SHELXTL-97*

software package [33,34]. Structures were checked for higher symmetry using PLATON [35]. All non-hydrogen atoms were located and refined anisotropically. Hydrogen atoms were placed in idealized locations and given isotropic thermal parameters equivalent to either 1.5 (terminal CH_3 hydrogen atoms) or 1.2 times the thermal parameter of the atom to which they were attached. Crystallographic data collection and refinement parameters are shown in Table 1. Crystals of **2**, obtained by vapor diffusion of water into a DMF solution, gave good quality data. No problems were encountered during the solution and refinement of this structure. Specific refinement details for **1** and **3** are described below.

Colorless plates of **1** were obtained by the slow evaporation of a DMF solution. All crystals screened displayed signs of non-merohedral twinning in the form of split reflections. After full data collection, the program CELL_NOW [36] was used to look for additional domains. Two domains were found that accounted for 97% of the harvested reflections. The second domain was rotated by 6.8° about the c^* axis. The data were integrated over both domains using SAINT [37]. An absorption correction was applied with the program TWINABS [38]. The corrected data were then analyzed for systematic absences and higher metric symmetry with XPREP [39] to determine the space group. The structure was solved with the SHELXTL-97 software package and refined using data from both domains. The second domain refined to a scale factor of 8.33%. Two molecules of **1** are present in the asymmetric unit in the space group $P\bar{1}$. Restraints on the directionality and size of the thermal displacement parameters of the nitrogen and carbon atoms of the ethylenediamine backbone of one of the molecules in the asymmetric unit were applied. The largest electron density peak and hole are 4.78 and −2.44 e Å^3, located 1.19 Å from Pt2 and 0.78 Å from Pt1, respectively. This large residual density might in part be due the presence of additional twin domains. It should also be noted that the space group utilized was $P\bar{1}$. Both β and γ are close to 90°, suggesting that a higher metric symmetry monoclinic space group might be more appropriate to describe the structure. Furthermore, the presence of two molecules of **1** in the asymmetric unit also raises concerns as to whether these two species are symmetry-related in a monoclinic space group. Structure solution in $P2_1/c$ gave basic atomic connectivity. During refinement, however, thermal ellipsoids attained unreasonable sizes and many became non-positive definite upon anisotropic refinement, a problem not encountered in $P\bar{1}$. Furthermore, the merging and refinement statistics and the standard deviations of the bond distances and angles for the $P2_1/c$ solution and refinement were substantially worse than those in the triclinic space group. The two molecules in the asymmetric unit in the $P\bar{1}$ solution exhibit only one obvious conformational difference. In particular, the tilting of the five-membered chelate rings is different, as discussed in more detail in Section 3.4. Searches for higher symmetry space groups with PLATON on the $P\bar{1}$ solution were unsuccessful.

X-ray quality crystals of **3** were grown by vapor diffusion of water into a DMF solution. The structure solved readily in $P2_12_12_1$. Unexpectedly, all four halide ligands refined best as bromine atoms. From additional characterization data presented in Sections 3.3 and 3.4, crystals of **3** are believed to be composed a disordered mixture of $[Pt(L)Cl_xBr_y]$ species, with site-occupancy disorder of chloride and bromide ligands present throughout. Despite several attempts, this type of disorder could not be successfully modeled. Hence, the Pt–Br distances in this structure should not be strictly interpreted as such.

2.8. Cell culture and cytotoxicity assays

HeLa cells grown as monolayers in Dulbecco's Modified Eagle Medium (DMEM) supplemented with 10% fetal bovine serum (FBS) and 1% penicillin/streptomycin were kept at 37 °C in a humidified incubator with 5% CO_2. Cells were passed every 3–4 days using stock solutions of trypsin/EDTA to detach the cells.

The cytotoxicities of **1**, **2**, and cisplatin were measured with the MTT assay. Cells were seeded in 96 well plates (2000 cells/well) and incubated for 16-24 h. The medium was then aspirated and replaced with 2-fold (for **1** and **2**) or 4-fold (for cisplatin) serial

Table 1
X-ray crystallographic data collection and refinement parameters.

	1	**2**	**3**
Formula	$C_{20}H_{26}Cl_2N_4O_2Pt$	$C_{20}H_{26}Cl_4N_4O_2Pt$	$C_{20}H_{26}Br_4N_4O_2Pt$
Formula weight	620.44	691.34	869.18
Space group	$P\bar{1}$	$P4_32_12$	$P2_12_12_1$
a (Å)	9.2382(10)	11.3811(3)	11.1850(5)
b (Å)	12.9438(14)		12.0391(6)
c (Å)	18.045(2)	18.4022(11)	18.2747(9)
α (°)	80.2930(17)		
β (°)	88.9920(18)		
γ (°)	90.0000(16)		
V (Å^3)	2126.5(4)	2383.63(17)	2460.8(2)
Z	4	4	4
ρ_{calc}, (g cm^{-3})	1.938	1.926	2.346
T (°C)	−173(2)	−173(2)	−173(2)
μ (Mo Kα), (mm^{-1})	6.874	6.360	12.222
θ range, (°)	1.60–25.06	2.10–28.71	2.03–29.13
Total no. of data	58892	50603	52226
No. of unique data	7479	3092	6631
No. of parameters	518	142	281
Completeness to θ (%)	99.4	99.9	100.0
R_1[a] (%)	8.00	2.42	5.42
wR_2[b] (%)	12.58	4.11	15.30
R_1[a] (%) for $I > 2\sigma$	4.93	1.92	5.03
wR_2[b] (%) for $I > 2\sigma$	11.07	4.11	14.95
Goodness-of-fit (GOF)[c]	1.024	1.058	1.095
Max, min peaks, (e Å^{-3})	4.783, −2.435	0.817, −0.558	3.799, −3.319
Flack parameter		−0.012(7)	−0.045(19)

[a] $R_1 = \sum ||F_o| - |F_c|| / \sum |F_o|$.

[b] $wR_2 = \{\sum[w(F_o^2 - F_c^2)^2] / \sum[w(F_o^2)^2]\}^{1/2}$.

[c] GOF $= \{\sum[w(F_o^2 - F_c^2)^2]/(n-p)\}^{1/2}$ where n is the number of data and p is the number of refined parameters.

dilutions of the desired platinum complex in growth medium. After a 72 h exposure time, the platinum-containing medium was removed and replaced with 200 μL of a solution of MTT (0.8 mg/mL) in serum-free DMEM. The MTT solution was aspirated after a 4 h incubation period, and the resulting purple formazan crystals were dissolved with a 3:80 v/v mixture of 35% aqueous ammonia and DMSO [40]. The absorbance in each well was read at 550 nm. The absorbance values were normalized to that of the untreated wells (100% cell viability) and plotted against compound concentration. The 50% growth inhibitory concentration (IC_{50}) values were estimated by interpolation of the resulting curves. The experiment was repeated at least in triplicate, using 6 wells per concentration level. Reported IC_{50} values are the averages derived from these independent experiments, and the errors are the resulting standard deviations. For **1** and **2**, the highest concentration levels utilized 0.2% DMF to solubilize the compounds. A control experiment revealed that the average cell viability after 72 h exposure to 0.2% pure DMF is 74 ± 6%. Therefore, the reported IC_{50} values of **1** and **2** are expected to be somewhat lower than those in the absence of the somewhat toxic DMF co-solvent.

3. Results and discussion

3.1. Synthesis and characterization of *1*

Previously, we reported that the dangling carboxylic acid of the platinum(II) complex, [Pt(edma)Cl_2] where edma = ethylenediamine-*N*-monoacetic acid, can engage in coupling reactions with amines to form stable amide bonds [22]. Inspired by this prior work, we investigated the amide coupling chemistry of the platinum complex [Pt(edda)Cl_2], where edda is ethylenediamine-*N*,*N*′-diacetic acid having two terminal carboxylic acid moieties. A suspension of [Pt(edda)Cl_2] in DMF was activated with 2 equiv of 1,1′-carbonyldiimidazole, resulting in a homogeneous yellow solution. The addition of benzylamine to the activated complex afforded complex **1**, [Pt(L)Cl_2] where L = ethylenediamine-*N*,*N*′-bis(*N*-benzylacetamide), as an off-white solid after appropriate workup (Scheme 1).

Formation of the amide bond was verified by IR spectroscopy, which revealed the disappearance of the free carboxylic acid stretching frequency near 1720 cm^{-1} of the starting material and concomitant formation of a C=O bond stretching frequency at 1662 cm^{-1}. Elemental analysis further verified the bulk composition of the isolated material. ESI-MS of **1**, in the negative ion mode, gave rise to three major ion peaks (Fig. S4, Supplementary data). In addition to the commonly observed $[M-H]^-$ and $[2\,M-H]^-$ peaks, the $[M-2H-Cl]^-$ peak was also detected.

NMR spectroscopy in DMF-d_7 revealed the presence of equal amounts of two species in solution. The ^{1}H NMR spectrum (Fig. S1, Supplementary data) shows two overlapping triplets centered at 8.64 ppm, which we assign to the NH proton of the newly formed amide bond. The NH resonances of the coordinated amines appear at 6.19 and 6.11 ppm. The ^{13}C NMR spectrum also shows a doubling of most of the signals expected for **1** (Fig. S2, Supplementary data). Two peaks in the ^{195}Pt NMR spectrum are observed at −2347 and −2362 ppm in an approximate 1:1 ratio (Fig. S3, Supplementary data). The small, 15 ppm difference between these signals suggests that the magnetic environments of platinum for the two species are very similar in solution. Because the coordinating nitrogen atoms of **1** are chiral, both the enantiomeric *R*,*R*/*S*,*S* and meso *R*,*S* diastereomers exist. The two distinct, yet chemically similar, species observed in solution are assigned as these two diastereomers.

3.2. Synthesis and characterization of *2*

The oxidation of **1** with $PhICl_2$ in DMF afforded the diaminotetrachloroplatinum(IV) complex, **2**, as the only product (Scheme 2). The IR data of **2** are similar to those of **1**, with the major C=O amide stretching frequency occurring at 1657 cm^{-1}. New Pt–Cl vibrational modes, which typically range between 300 and 400 cm^{-1}, could not be observed within the window of the spectrometer used (4000–400 cm^{-1}). The ESI-MS of **2** in the negative ion mode displays peaks for the $[M-H]^-$ and $[2\,M-H]^-$ ions, confirming the presence of the two newly introduced chlorine atoms (Fig. S8, Supplementary data). Three other significant peaks due to the $[M-2H-Cl]^-$, $[M-3H-2Cl]^-$, and $[M-4H-3Cl]^-$ ions were present as well, corresponding to sequential loss of chloride anions and protons from the parent fragment.

As for **1**, two distinct species are present in solution that we assign to analogous *R*,*R*/*S*,*S* and *R*,*S* diastereomers. For **2** in DMF, however, the ratio of these two species is approximately 1:3, in contrast to the 1:1 ratio observed for **1**. The NH resonances of the coordinated amine ligand in the ^{1}H NMR spectrum (Fig. S5, Supplementary data) are shifted downfield relative to those of **1** and are largely obscured by overlapping resonances of the aromatic protons. This overlap prevents observation of ^{195}Pt coupling to the NH protons, typically observed for platinum(IV) complexes. The major diastereomer resonates at −378 ppm in the ^{195}Pt NMR spectrum, whereas the minor diastereomer resonates at −370 ppm (Fig. S7, Supplementary data). The significant downfield shift (≈2000 ppm) of the ^{195}Pt NMR resonances of **2** relative to those of **1** is expected on the basis of the greater platinum oxidation state of **2** (+4) in comparison to **1** (+2). The ^{195}Pt NMR chemical shifts of **2** are similar to those of a related $Pt^{IV}N_2Cl_4$ complex [22].

3.3. Oxidation of *1* with Br_2

Treatment of **1** as a suspension in DMF with 1.5 equiv of Br_2 led to the formation of a homogeneous orange solution. Slow diffusion of water vapor into this solution afforded orange microcrystalline material. Analysis of the product by ESI-MS revealed an envelope of molecular ion peaks (Fig. S10, Supplementary data). A peak corresponding to the ion of the expected Br_2 oxidative addition product, $[PtLCl_2Br_2-H]^-$, was observed at *m*/*z* 778.8 (Calc. 778.9). In addition, eight other peaks corresponding to the ions, $[PtLCl_{2-n}Br_{2-m}-nCl-mBr-(1+m+n)H]^-$ where n and m are integers under the condition m + n ≤3 were detected. These species are analogous to the $[PtLCl_4-2H-Cl]^-$, $[PtLCl_4-3H-2Cl]^-$, and $[PtLCl_4-4H-3Cl]^-$ ions observed for **2**, and arise from different combinations of Cl^- and Br^- loss upon ionization. A peak at *m*/*z* 734.8 corresponds to

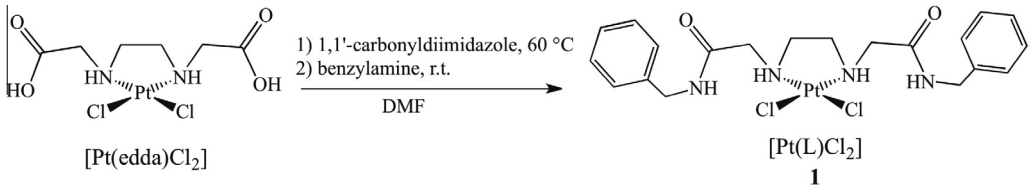

Scheme 1. Synthesis of compound **1**.

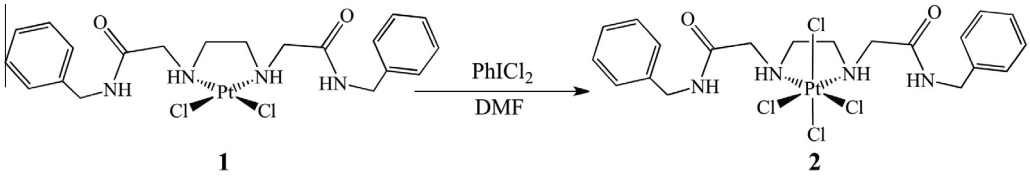

Scheme 2. Synthesis of compound **2**.

the ion $[PtLCl_3Br–H]^-$ (Calc. 735.0), and a peak at 822.7 is assigned to the species $[PtLClBr_3–H]^-$ (Calc. 822.9). A signal at *m/z* 904.7 could correspond either to $[PtLClBr_3+Br]^-$ or $[PtLBr_4+Cl]^-$ (Calc. for both 904.8). These latter three peaks indicate that partial intermolecular halide exchange might occur either in solution or gas-phase, giving rise to core fragments with the unexpected $PtLCl_3Br$, $PtLClBr_3$, and $PtLBr_4$ molecular formulae.

The ^{1}H NMR spectrum of this material (Fig. S9, Supplementary data) displays a broad multiplet centered at 8.90 ppm, which is assigned to the NH amide resonance. Two distinct triplets, as observed for **1** and **2**, could not be clearly resolved from this signal. With the exception of a sharp doublet at 4.50 ppm assigned to the benzyl CH_2 group, the aliphatic region shows a series of poorly overlapping multiplets ranging from 4.8 to 3.2 ppm. Therefore, the ^{1}H NMR spectrum is indicative of more than just two species present in solution.

Investigation of the solution ^{195}Pt NMR spectrum of this material confirmed the presence of multiple platinum-containing compounds. At least seven different species are observed in the ^{195}Pt NMR spectrum. The ^{195}Pt chemical shifts of these compounds range from −599 to −1425 ppm (Fig. 1). These peaks are hypothesized to arise from a mixture of $[Pt(L)Cl_xBr_{x-4}]$ compounds with different ratios of bromide and chloride ligands. The peak at −1425 ppm is similar to those of the tetrabromide compounds, $[Pt(en)Br_4]$ (δ = −1473 ppm) [41], [Pt(*trans*-1,2-diaminocyclohexane)Br_4] (δ = −1525 ppm) [42], and [Pt(*cis*-1,2-diamoncyclohexane)Br_4] (δ = −1540 ppm) [42], and it is therefore assigned to the species, $[Pt(L)Br_4]$. The cluster of peaks ranging from −878 to −933 ppm fall in a region expected for platinum(IV) compounds with an $N_2Cl_2Br_2$ coordination sphere. For example, the compounds *cis*,*cis*,*trans*-$[Pt(NH_3)_2Cl_2Br_2]$, *cis*,*trans*-[Pt(*trans*-1,2-diaminocyclohexane)Cl_2Br_2], and *cis*,*trans*-[Pt(*cis*-1,2-diaminocyclohexane)Cl_2Br_2] resonate at −980, −976, and −990 ppm, respectively [42,43]. The observation of several peaks in this region most likely derives from a mixture of cis and trans isomers and diastereomers owing to the chirality of the coordinating nitrogen atoms. The peaks at −599 and −647 ppm are tentatively assigned to different isomers of the complex, $[Pt(L)Cl_3Br]$, whereas the peaks between −1120 and −1175 ppm are assigned to isomers of $[Pt(L)ClBr_3]$. Although, to the best of our knowledge, ^{195}Pt NMR data for platinum(IV) complexes with similar N_2Cl_3Br and N_2ClBr_3 coordination spheres have not been reported, the positions of these peaks are consistent with the ability of softer ligands, such as bromide, to systematically shift the ^{195}Pt NMR resonance upfield [44]. In comparing the ^{195}Pt chemical shifts for the N_2Cl_4 complex **2** and the species observed here, it appears that sequential substitution of a chloride for a bromide ligand leads to an upfield shift of 250–300 ppm. Similarly, the ^{195}Pt NMR chemical shift of the $[PtBr_6]^{2-}$ anion moves upfield by approximately 290 ppm for each replacement of a chloride for a bromide ligand [45]. The precise mechanism by which these mixed halide species form remains uncertain. The presence of a small amount of unreacted platinum(II) starting material may facilitate halide scrambling via the well known platinum(II)-catalyzed ligand substitution reactions of platinum(IV) complexes [46].

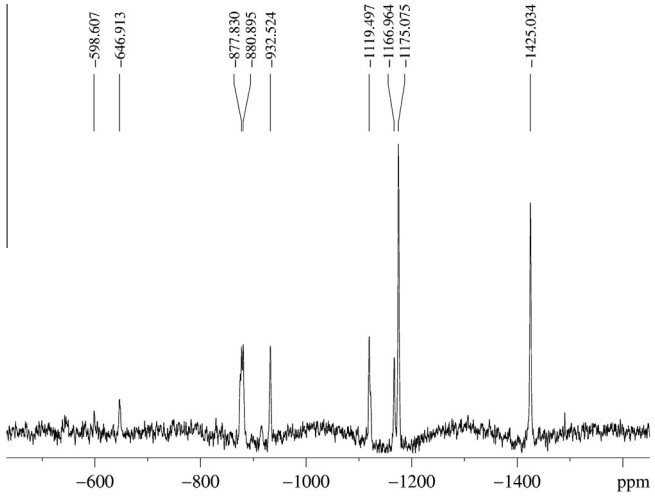

Fig. 1. ^{195}Pt NMR spectrum of the Br_2-oxidation products of **1** in DMF-d_7. A small degree of baseline rolling is observed, most likely due to acoustic ringing of the probe.

3.4. Description of crystal structures

Two molecules of **1** crystallize in the asymmetric unit. One of these molecules is depicted in Fig. 2, and selected bond distances and angles are collected in Table 2. The other molecule is shown in the Supplementary data (Fig. S11), along with bond distances and angles (Table S1). The platinum atom has square-planar coordination, as expected for this ion in the +2 oxidation state. The two non-symmetry related molecules are *meso*-*R*,*S* diastereomers as conveyed by their nitrogen centers. A significant difference between them is the canting of the five-membered chelate ring. The conformation of non-planar five-membered chelate rings produces two different chiral orientations of the ligand, referred to as λ and δ (Fig. 3) [47]. One of the molecules in the asymmetric unit has the λ chelate ring conformation, whereas the other displays a δ chelate ring conformation. No disorder occurs in the ethylenediamine backbone, confirming that the two molecules are crystallographically distinct and not symmetry related.

Complex **2** crystallizes in the chiral space group, $P4_32_12$ with half a molecule per asymmetric unit. The platinum center lies on a crystallographic 2-fold symmetry axis. Complex **2** attains the expected octahedral coordination geometry for a platinum(IV) ion, as shown in Fig. 4. The Pt-ligand bond lengths and angles are typical for this oxidation state and geometry and are summarized in Table 3. The 2-fold axis requires that both coordinating nitrogen atoms attain the same stereochemistry, and for the crystal studied the complex is the *S*,*S* enantiomer. The fact that the Flack parameter refined to a value near zero confirms this choice. Crystals with the *R*,*R* enantiomer presumably comprise half of the sample. The conformation of the chelate ring is δ.

Orange crystals obtained from the oxidation of **1** with Br_2 were analyzed by X-ray diffraction. A structure solution was obtained using the non-centrosymmetric space group $P2_12_12_1$. Despite the decrease in symmetry from tetragonal to orthorhombic, the unit cell parameters are similar to those of **2** with *a* between 11 and

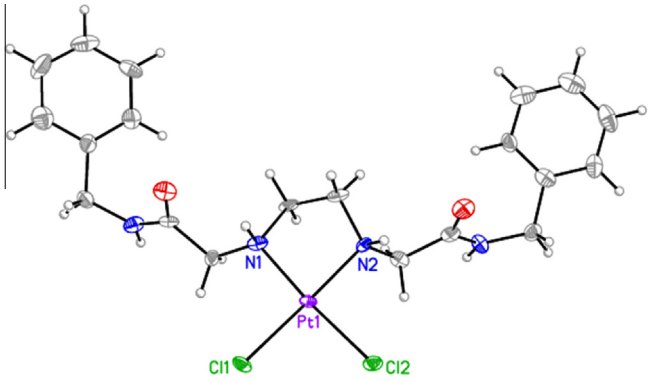

Fig. 2. Structure of one of the molecules of **1** in the asymmetric unit. Thermal ellipsoids are drawn at the 50% probability level.

Table 2
Selected interatomic distances (Å) and angles (degrees) for one of the molecules of **1** in the asymmetric unit.[a]

Bonds		Angels	
Pt1–N1	2.060(8)	N1–Pt1–N2	84.3(3)
Pt1–N2	2.061(8)	N1–Pt1–Cl1	94.1(2)
Pt1–Cl1	2.310(2)	N1–Pt1–Cl2	175.2(2)
Pt1–Cl2	2.303(2)	N2–Pt1–Cl1	178.3(2)
		N2–Pt1–Cl2	90.9(2)
		Cl1–Pt1–Cl2	90.74(9)

[a] Atoms are labeled as indicated in Fig. 2. Numbers in parentheses are the estimated standard deviations of the last significant figures.

12 Å and c near 18.3 Å. The structure, solved and refined successfully as [Pt(L)Br_4] (**3**), is depicted in Fig. 5. The expected octahedral coordination geometry for platinum(IV) is attained. Bond lengths and angles are collected in Table 4. The perfect 2-fold symmetry of **2** is not observed for **3** owing to a difference in the orientation of a benzyl-amide ligand arm. The complex resolves in the solid-state as the *R*,*R* enantiomer with a λ conformation of the five-membered chelate ring.

Table 3
Selected interatomic distances (Å) and angles (degrees) for **2**.[a]

Bonds		Angles			
Pt1–N1	2.083(2)	N1–Pt1–N1A	84.28(14)	N1–Pt1–Cl2A	92.79(7)
Pt1–Cl1	2.3091(7)	N1–Pt1–Cl1	89.69(8)	Cl1–Pt1–Cl2	90.21(4)
Pt1–Cl2	2.3061(7)	N1–Pt1–Cl2	177.07(7)	Cl1–Pt1–Cl1A	177.15(5)
		N1–Pt1–Cl1A	88.20(8)	Cl2–Pt1–Cl2A	90.14(4)

[a] Atoms are labeled as indicated in Fig. 4. Numbers in parentheses are the estimated standard deviations of the last significant figures.

The structure of [Pt(L)Br_4] was somewhat unexpected. By ^{195}Pt NMR spectroscopy, a number of different species, corresponding to different ratios of bromide and chloride ligands on the platinum(IV) center, were discovered to comprise the bulk microcrystalline material isolated from the oxidation of **1** with Br_2. We considered the hypothesis that the X-ray structure solution might correspond to a homogeneous compound such as the tetrabromide complex that serendipitously separated from the other species by fractional crystallization. An X-ray powder pattern of the bulk orange microcrystalline material, however, is in substantial agreement with that of the computed pattern of **3** with only minor deviations of the intensities at $2\theta \geq 20°$. These differences might reflect the presence of a small number of impurities (Fig. 6). These impurities might correspond to crystallites of other mixed halide species in the mixture, as suggested by mass spectrometry and platinum NMR spectroscopy. In addition, refinement of **3** resulted in thermal parameters for the bromide ligands greater than that of the platinum atom and in violation of the Hirshfeld rigid-bond test [48], consistent with site-position disorder involving lighter

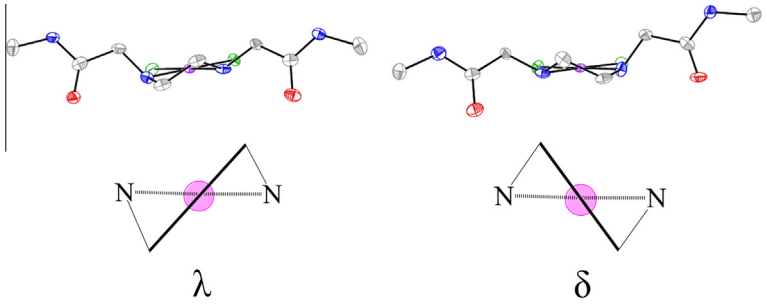

Fig. 3. Depiction of the λ and δ isomers of **1** found in the asymmetric unit. Hydrogen atoms and phenyl rings are omitted for clarity.

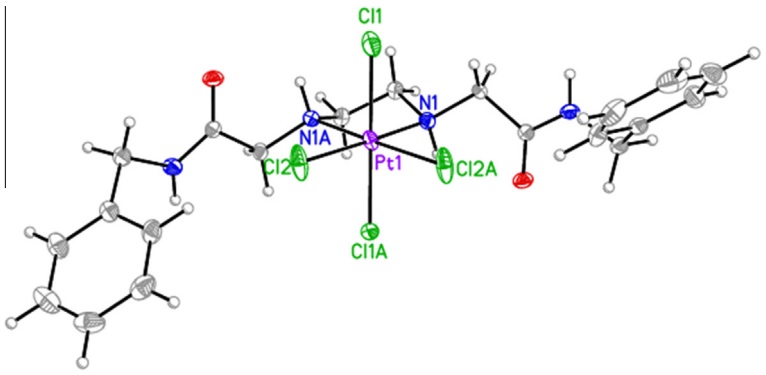

Fig. 4. Structure of **2**. Thermal ellipsoids are drawn at the 50% probability level.

atoms. The Pt–Br distances determined from the crystal structure of the related complex, [Pt(en)Br_4], are 2.461(2) and 2.488(2) Å for the axial and equatorial positions, respectively [41]. For **3**, the Pt–Br distances are systematically shorter, ranging from 2.3934(15) to 2.4359(15) Å. These shorter Pt–Br distances are most likely a consequence of unresolved substitutional disorder of bromide and chloride ligands. Although **3** refined satisfactorily as [Pt(L)Br_4], the powder diffraction, ^{195}Pt NMR spectroscopic and ESI-MS results all argue in favor of a disordered superposition of halo species. Accordingly, the Pt–Br distances derived from this data set should be interpreted with caution.

3.5. DFT calculations

The relative thermodynamic stabilities of the two diastereomers (*R*,*R*/*S*,*S* and *R*,*S*) of **1** and **2** were investigated by DFT calculations. These diastereomers were optimized in the gas-phase. The optimized structures are shown in the Supplementary data (Figs. S12–S15), where their Cartesian coordinates are also deposited (Tables S2–S5). The calculated Gibbs free energy difference at 298 K between the *S*,*S* and *R*,*S* diastereomers of **1** is 0.32 kcal/mol, whereas for the diastereomers of **2**, the energy difference is 1.09 kcal/mol. For both **1** and **2**, the *S*,*S* diastereomer is computed to be the thermodynamically preferred isomer, although these energy differences are within the error of the DFT calculations. The small energy differences, which correspond to equilibrium constants of 1.7 and 6.3 for **1** and **2**, respectively, are consistent with the observation of both species in solution by NMR spectroscopy. For a series of similar platinum(II) and platinum(IV) complexes bearing related ethylenediamine-*N*,*N*′-diester ligands, computed energy differences between diastereomers are on the order of several kcal/mol, thereby explaining the observation of only one of the isomers in solution by NMR spectroscopy [49–53].

3.6. Cytotoxicity measurements

The antiproliferative effects of **1**, **2**, and cisplatin as a control were determined in HeLa cells by the MTT assay. The 50% growth inhibitory concentration (IC_{50}) values are collected in Table 5. Both

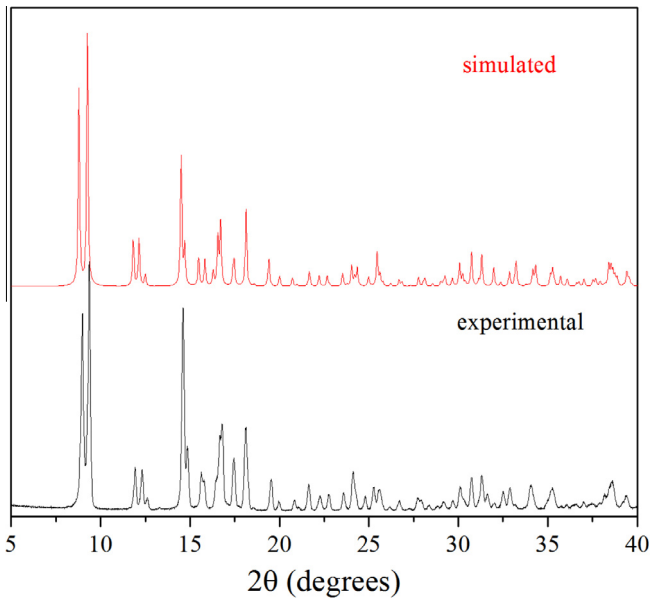

Fig. 6. X-ray powder diffraction pattern of the bulk material isolated from the oxidation of **1** with Br_2 (bottom, black), along with the simulated diffraction powder from the single crystal structure **3** (top, red). (For interpretation of the references to colour in this figure legend, the reader is referred to the web version of this article.)

1 and **2** are more than order of magnitude less cytotoxic than cisplatin, with IC_{50} values of approximately 50 μM. The fact that both complexes exhibit identical IC_{50} values is not unexpected because *cis*-diaminetetrachloroplatinum(IV) complexes are rapidly reduced to their platinum(II) analogs by a variety of biologically relevant reducing agents [54–56]. Tetraplatin, a related platinum(IV) complex with an N_2Cl_4 coordination sphere, is reduced within 15 min in RPMI cell growth medium [57]. Therefore, for **2**, reduction most likely also occurs in the growth medium prior to internalization by the cells. The low in vitro cytotoxicities of **1** and **2** measured here suggest that these complexes are poor anticancer drug candidates. In contrast, several of the aforementioned platinum(II) and

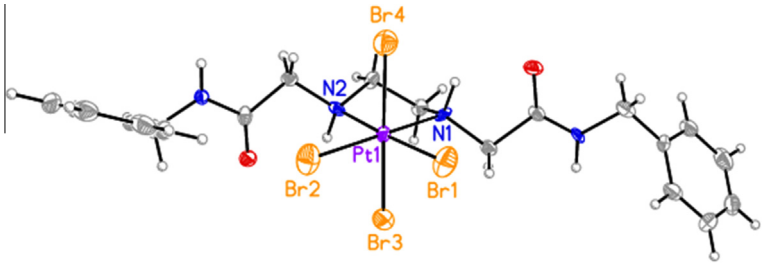

Fig. 5. Structure of **3**. Thermal ellipsoids are drawn at the 50% probability level.

Table 4
Selected interatomic distances (Å) and angles (degrees) for **3**.[a]

Bonds		Angles					
Pt1–N1	2.101(9)	N1–Pt1–N2	83.9(3)	N2–Pt1–Br2	92.9(2)	Br2–Pt1–Br3	89.64(6)
Pt1–N2	2.103(9)	N1–Pt1–Br1	92.6(3)	N2–Pt1–Br3	89.2(2)	Br2–Pt1–Br4	93.02(6)
Pt1–Br1[b]	2.3988(15)	N1–Pt1–Br2	176.4(3)	N2–Pt1–Br4	89.2(2)	Br3–Pt1–Br4	176.95(6)
Pt1–Br2[b]	2.3934(15)	N1–Pt1–Br3	88.5(2)	Br1–Pt1–Br2	90.57(6)		
Pt1–Br3[b]	2.4197(14)	N1–Pt1–Br4	88.8(2)	Br1–Pt1–Br3	91.92(6)		
Pt1–Br4[b]	2.4359(15)	N2–Pt1–Br1	176.3(2)	Br1–Pt1–Br4	89.54(6)		

[a] Atoms are labeled as indicated in Fig. 5. Numbers in parentheses are the estimated standard deviations of the last significant figures.
[b] These distances are shorter than anticipated owing to partial occupancy of the site by chloride (see text).

Table 5
IC_{50} values of cisplatin, **1**, and **2** in HeLa cells.[a]

Compound	IC_{50} (μM)
Cisplatin	1.0 ± 0.8
1	50 ± 2
2	47 ± 11

[a] Reported errors are standard deviations of at least three independent experiments.

platinum(IV) complexes with ethylenediamine-*N*,*N*′-diester ligands exhibit IC_{50} values of less than 20 μM in several cell lines [50–53,58,59]. The reasons for the lower cytoxicities of **1** and **2** relative to these complexes and cisplatin remain to be determined.

4. Summary and conclusions

The platinum(II) complex, [Pt(edda)Cl_2], can be readily coupled through amide bond formation at the two non-coordinating carboxylic acid moieties of the edda ligand, as demonstrated here in the synthesis of **1** from benzyl amine. The oxidation of **1** with $PhICl_2$ cleanly afforded the tetrachloro platinum(IV) complex **2**, whereas oxidation by Br_2 yielded a mixture of platinum(IV) complexes with different ratios of bromide and chloride ligands. The antiproliferative properties of **1** and **2** are the same, independent of the platinum oxidation state. Although both are significantly less cytotoxic than cisplatin, the convenient amide coupling chemistry employed for their synthesis could be used to access many different derivatives, some of which may show improved activity. This chemistry will be of general use in the future design of novel platinum anticancer drug candidates.

Acknowledgements

This work was supported by Grant CA034992 from the National Cancer Institute. Spectroscopic instrumentation at the MIT DCIF is maintained with funding from NIH Grant 1S10RR13886-01. J.J.W. is the recipient of a David H. Koch Graduate Fellowship. The authors thank Mr. Carl Brozek and Professor Mircea Dincă for assistance with and use of a powder X-ray diffractometer, and Mr. Timothy Johnstone and Dr. Patricia Marqués-Gallego for comments on the manuscript.

Appendix A. Supplementary data

CCDC 889358, 889359, and 889360 contain the supplementary crystallographic data for **1**, **2** and **3**. These data can be obtained free of charge via http://www.ccdc.cam.ac.uk/conts/retrieving.html, or from the Cambridge Crystallographic Data Centre, 12 Union Road, Cambridge CB2 1EZ, UK; fax: +44 1223 336 033; or e-mail: deposit@ccdc.cam.ac.uk. Supplementary data associated with this article can be found, in the online version, at http://dx.doi.org/10.1016/j.poly.2012.07.097.

References

[1] L. Kelland, Nat. Rev. Cancer 7 (2007) 573.
[2] K.S. Lovejoy, S.J. Lippard, Dalton Trans. (2009) 10651.
[3] G. Daugaard, U. Abildgaard, Cancer Chemother. Pharmacol. 25 (1989) 1.
[4] D. Screnci, M.J. McKeage, J. Inorg. Biochem. 77 (1999) 105.
[5] L. Galluzzi, L. Senovilla, I. Vitale, J. Michels, I. Martins, O. Kepp, M. Castedo, G. Kroemer, Oncogene 31 (2012) 1869.
[6] K.R. Barnes, A. Kutikov, S.J. Lippard, Chem. Biol. 11 (2004) 557.
[7] M. Reithofer, M. Galanski, A. Roller, B.K. Keppler, Eur. J. Inorg. Chem. (2006) 2612.
[8] M.R. Reithofer, S.M. Valiahdi, M.A. Jakupec, V.B. Arion, A. Egger, M. Galanski, B.K. Keppler, J. Med. Chem. 50 (2007) 6692.
[9] M.R. Reithofer, A. Schwarzinger, S.M. Valiahdi, M. Galanski, M.A. Jakupec, B.K. Keppler, J. Inorg. Biochem. 102 (2008) 2072.
[10] M.R. Reithofer, A.K. Bytzek, S.M. Valiahdi, C.R. Kowol, M. Groessl, C.G. Hartinger, M.A. Jakupec, M. Galanski, B.K. Keppler, J. Inorg. Biochem. 105 (2011) 46.
[11] H. Varbanov, S.M. Valiahdi, A.A. Legin, M.A. Jakupec, A. Roller, M. Galanski, B.K. Keppler, Eur. J. Med. Chem. 46 (2011) 5456.
[12] S. Mukhopadhyay, C.M. Barnés, A. Haskel, S.M. Short, K.R. Barnes, S.J. Lippard, Bioconjugate Chem. 19 (2008) 39.
[13] S. Abramkin, S.M. Valiahdi, M.A. Jakupec, M. Galanski, N. Metzler-Nolte, B.K. Keppler, Dalton Trans. 41 (2012) 3001.
[14] L. Gaviglio, A. Gross, N. Metzler-Nolte, M. Ravera, Metallomics 4 (2012) 260.
[15] N. Graf, T.E. Mokhtari, I.A. Papayannopoulos, S.J. Lippard, J. Inorg. Biochem. 110 (2012) 58.
[16] R.P. Feazell, N. Nakayama-Ratchford, H. Dai, S.J. Lippard, J. Am. Chem. Soc. 129 (2007) 8438.
[17] S. Dhar, Z. Liu, J. Thomale, H. Dai, S.J. Lippard, J. Am. Chem. Soc. 130 (2008) 11467.
[18] S. Dhar, W.L. Daniel, D.A. Giljohann, C.A. Mirkin, S.J. Lippard, J. Am. Chem. Soc. 131 (2009) 14652.
[19] K.M.L. Taylor-Pashow, J.D. Rocca, Z. Xie, S. Tran, W. Lin, J. Am. Chem. Soc. 131 (2009) 14261.
[20] H.T.T. Duong, V.T. Huynh, P. de Souza, M.H. Stenzel, Biomacromolecules 11 (2010) 2290.
[21] Y. Min, C. Mao, D. Xu, J. Wang, Y. Liu, Chem. Commun. 46 (2010) 8424.
[22] J.J. Wilson, S.J. Lippard, Inorg. Chim. Acta 389 (2012) 77.
[23] J.N. Jolley, A.I. Yanovsky, L.R. Kelland, K.B. Nolan, J. Inorg. Biochem. 83 (2001) 91.
[24] X.-F. Zhao, C. Zhang, Synthesis (2007) 551.
[25] F. Neese, ORCA, an Ab Initio Density Functional and Semiempirical Electronic Structure Program Package, Universität Bonn, Bonn, Germany, 2010.
[26] A.D. Becke, J. Chem. Phys. 84 (1986) 4524.
[27] J.P. Perdew, W. Yue, Phys. Rev. B 33 (1986) 8800.
[28] J.P. Perdew, Phys. Rev. B 33 (1986) 8822.
[29] D.A. Pantazis, X.-Y. Chen, C.R. Landis, F. Neese, J. Chem. Theory Comput. 4 (2008) 908.
[30] F. Weigend, R. Ahlrichs, Phys. Chem. Chem. Phys. 7 (2005) 3297.
[31] APEX2, Bruker AXS, Inc., Madison, WI, 2008.
[32] G.M. Sheldrick, SADABS: Area-detector Absorption Correction, University of Göttingen, Göttingen, Germany, 2008.
[33] G.M. Sheldrick, SHELXTL-97, University of Göttingen, Göttingen, Germany, 2000.
[34] G.M. Sheldrick, Acta Crystallogr. Sect. A 64 (2008) 112.
[35] A.L. Spek, PLATON, A Multipurpose Crystallographic Tool, Utrecht University, Utrecht, The Netherlands, 2008.
[36] G.M. Sheldrick, CELL_NOW, University of Göttingen, Göttingen, Germany, 2008.
[37] SAINT: SAX Area-Detector Integration Program, Bruker AXS, Inc., Madison, WI, 2009.
[38] G.M. Sheldrick, TWINABS, University of Göttingen, Göttingen, Germany, 2008.
[39] XPREP, Bruker AXS, Inc., Madison, WI, 2008.
[40] H. Wang, F. Wang, X. Tao, H. Cheng, Anal. Biochem. 421 (2012) 324.
[41] K. Hindmarsh, D.A. House, M.M. Turnbull, Inorg. Chim. Acta 257 (1997) 11.
[42] S. Al-baker, Z.H. Siddik, A.R. Khokhar, J. Coord. Chem. 31 (1994) 109.
[43] R.J. Brandon, J.C. Dabrowiak, J. Med. Chem. 27 (1984) 861.
[44] P.S. Pregosin, Coord. Chem. Rev. 44 (1982) 247.
[45] S.J.S. Kerrison, P.J. Sadler, J. Magn. Reson. 31 (1978) 321.
[46] W.R. Mason, Coord. Chem. Rev. 7 (1972) 241.
[47] K.A. Jensen, Inorg. Chem. 9 (1970) 1.
[48] F.L. Hirshfeld, Acta Crystallogr. Sect. A 32 (1976) 239.
[49] G.N. Kaluđerović, H. Schmidt, S. Schwieger, C. Wagner, R. Paschke, A. Dietrich, T. Mueller, D. Steinborn, Inorg. Chim. Acta 361 (2008) 1395.
[50] G.N. Kaluđerović, H. Kommera, S. Schwieger, A. Paethanom, M. Kunze, H. Schmidt, R. Paschke, D. Steinborn, Dalton Trans. (2009) 10720.
[51] J.M. Lazić, L. Vučićević, S. Grgurić-Šipka, K. Janjetović, G.N. Kaluđerović, M. Misirkić, M. Gruden-Pavlović, D. Popadić, R. Paschke, V. Trajković, T.J. Sabo, Chem. Med. Chem. 5 (2010) 881.
[52] J.M. Vujić, G.N. Kaluđerović, M. Milovanović, B.B. Zmejkovski, V. Volarević, D. Živić, P. Đurđević, N. Arsenijević, S.R. Trifunović, Eur. J. Med. Chem. 46 (2011) 4559.
[53] J.M. Vujić, G.N. Kaluđerović, B.B. Zmejkovski, M. Milovanović, V. Volarević, N. Arsenijević, T.P. Stanojković, S.R. Trifunović, Inorg. Chim. Acta 390 (2012) 123.
[54] S. Choi, C. Filotto, M. Bisanzo, S. Delaney, D. Lagasee, J.L. Whitworth, A. Jusko, C. Li, N.A. Wood, J. Willingham, A. Schwenker, K. Spaulding, Inorg. Chem. 37 (1998) 2500.
[55] K. Lemma, J. Berglund, N. Farrell, L.I. Elding, J. Biol. Inorg. Chem. 5 (2000) 300.
[56] K. Lemma, D.A. House, N. Retta, L.I. Elding, Inorg. Chim. Acta 331 (2002) 98.
[57] G.R. Gibbons, S. Wyrick, S.G. Chaney, Cancer Res. 49 (1989) 1402.
[58] G.N. Kaluđerović, V.M. Đinović, Z.D. Juranić, T.P. Stanojković, T.J. Sabo, J. Inorg. Biochem. 99 (2005) 488.
[59] B.B. Krajčinović, G.N. Kaluđerović, D. Steinborn, H. Schmidt, C. Wagner, Ž. Žižak, Z.D. Juranić, S.R. Trifunović, T.J. Sabo, J. Inorg. Biochem. 102 (2008) 892.